SAND98-2512J

JOURNAL OF MATERIALS SCIENCE: MATERIALS IN ELECTRONICS (submitted 1998)

# Reciprocal-space analysis of compositional modulation in short-period superlattices using position-sensitive x-ray detection

S. R. LEE, J. MIRECKI MILLUNCHICK[a], R. D. TWESTEN[b], D. M. FOLLSTAEDT, J. L. RENO
*Sandia National Laboratories, Albuquerque, NM, USA 87185-0601*

S. P. AHRENKIEL, A. G. NORMAN
*National Renewable Energy Laboratory, Golden, CO, USA 80401-3393*

[a] *Now at the Department of Materials Science and Engineering, University of Michigan, Ann Arbor, MI 48109-2136*
[b] *Now at the Center for Microanalysis of Materials, University of Illinois, Urbana, IL 61801-2985*

---

Epitaxial growth of AlAs-InAs short-period superlattices on (001) InP can lead to heterostructures exhibiting strong, quasi-periodic, lateral modulation of the alloy composition; transverse satellites arise in reciprocal space as a signature of the compositional modulation. Using an x-ray diffractometer equipped with a position-sensitive x-ray detector, we demonstrate reciprocal-space mapping of these satellites as an efficient, nondestructive means for detecting and characterizing the occurrence of compositional modulation. Systematic variations in the compositional modulation due to the structural design and the growth conditions of the short-period superlattice are characterized by routine mapping of the lateral satellites.

## 1. Introduction

Molecular-beam epitaxy (MBE) of short-period superlattices (SPSs) often leads to heterostructures with unintended lateral variations in the alloy composition. Particularly strong and regular compositional modulation arises for growth of nominally lattice-matched SPSs having periods near four monolayers (ML). This growth-induced modulation was first observed by Hsieh et al. at the University of Illinois in 1990 for $(GaP)_{2ML}(InP)_{2ML}$ superlattices grown on (001) GaAs [1]. In 1992, the Illinois group reported the same effect for growth of $(GaAs)_{2ML}(InAs)_{2ML}$ superlattices on (001) InP [2]. More recently, we have observed compositional modulation for growth of $(AlAs)_{2ML}(InAs)_{2ML}$ superlattices on (001) InP [3].

In these SPS structures, the local binary-alloy mole fractions can vary laterally by more than ±0.1 about the nominal average value of 0.5 [1, 4, 5]; the wavelength of the modulations is typically 10-40 nm [1-4]. Depending upon the alloy system, the lateral modulation can be either one-dimensional [6,7] or two-dimensional [5,8,9] in character. One-dimensional (1-D) modulation in SPSs grown to thicknesses equal to the lateral wavelength produces wire-like domains, while two-dimensional (2-D) modulation produces box- or dot-like domains. In thicker SPSs the modulated domains may continuously self-align vertically; 1-D wire-like domains elongate along the growth direction to form sheet-like domains or lateral quantum wells. Similarly, 2-D dot-like domains elongate to form columns.

In all cases, the lateral modulation superimposes on a remnant of the intended SPS modulation; fundamental modifications of the bandstructure and optoelectronic properties of the ideal SPS accompany the lateral modulation of the alloy composition [10]. Quantum-wire-based lasers [11] and lateral-superlattice solar cells [12], which take advantage of the novel materials properties and microstructures produced by lateral modulation of the alloy composition, are being pursued. Understanding and control of this spontaneous phenomenon, as a means of producing novel devices and also as a means of eliminating compositional modulation as an unwanted parasitic effect, are clearly desirable from a technological point of view. While various phenomenological [13], thermodynamic-ground-state [14-17], and kinetic-thermodynamic-instability models [18, 19] have been proposed which may explain compositional modulation; demonstrated comprehensive understanding of the physical processes producing unintended compositional modulation during SPS growth remains elusive [20].

Consequently, determination of the SPS structures and growth conditions that optimize compositional modulation for a specific purpose is still largely an experimental undertaking. Transmission electron microscopy (TEM) is the long-standing tool of choice for detecting, studying, and optimizing compositional modulation; but TEM requires labor-intensive sample preparation and is difficult to use for routine examination of numerous samples. An alternative means of characterization arises from the quasi-periodic character of the lateral modulation. This lateral superstructure creates corresponding lateral satellites in reciprocal space that may be nondestructively analyzed by x-ray diffraction. The present paper reports our efforts to broadly apply x-ray diffraction reciprocal-space mapping to the study of lateral compositional modulation in $(AlAs)_m(InAs)_n$ SPSs grown on (001) InP.

## 2. The reciprocal-space structure of compositionally modulated SPSs

The power of reciprocal-space mapping in two-dimensions arises in a singular way: by breaking the perfect in-plane homogeneity of the layered epitaxial single-crystal through the introduction of lateral structure. Consider first a laterally perfect crystal comprised of individual lamellae that are each laterally homogenous; all structural variations occur normal to the lamellae – an example would be an ideally coherent conventional superlattice grown on a singular substrate. The real-space structure along the surface-normal direction appears in reciprocal space as a corresponding elongation of the reciprocal-lattice points into extended, modulated rods oriented normal to the lamellae forming the crystal. Conventional, one-dimensional, x-ray rocking curves basically map the diffracted intensity distributions that arise along these rods. If the lamellae are laterally perfect, the entire local structure of reciprocal space is known from the rocking curve.

Now, consider what happens when we break the in-plane perfection of the layered crystal by inserting defects (e.g., dislocations, stacking faults, voids, or precipitates), microstructures (e.g., quantum-dot or wire arrays, surface morphology, or interface roughness), or lateral compositional fluctuations (e.g., phase-separated or atomically ordered domains). Insertion of these laterally finite structures produces lamellae that are now inhomogeneous along the in-plane direction. Lateral in-plane structure in real-space leads directly to corresponding lateral structure in reciprocal space. This lateral structure is seen in x-ray diffraction experiments as a three-dimensional distribution of diffuse x-ray scattering into regions of reciprocal space laterally adjacent to the positions of the crystal-truncation rods. The basic purpose of reciprocal-space mapping is to measure the detailed three-dimensional structure that arises when lateral inhomogeneity is introduced into the crystal. Ideally, one desires a complete three-dimensional (3-D) map of the diffracted intensity in reciprocal space; however, instrumental considerations dictate otherwise. Typical reciprocal-space maps are 2-D projections of a finite-thickness slice of the 3-D reciprocal space. Proper interpretation of reciprocal-space maps (and rocking-curves, as well) often requires an awareness of this embedded three-dimensional character.

Lateral compositional modulation in short-period superlattices is but one specific type of lateral inhomogeneity that can be studied by mapping of its corresponding structure in reciprocal space. The microstructure of the 1-D lateral compositional modulation originally found in both $(GaP)_m(InP)_n$ and $(GaAs)_m(InAs)_n$ SPSs is illustrated in Figure 1(a). Figure 1(b) shows a $[\bar{1}10]$ zone-axis view of the corresponding reciprocal-space structure. The lateral superstructure in real-space produces corresponding lateral satellites about each reciprocal-lattice point. The lateral [110] separation of the satellites produced by the compositional modulation is $2\pi/p_{cm}$, where $p_{cm}$ is the period of the lateral modulation. As depicted in Figure 1(a), the intended surface-normal SPS modulation partially survives the onset of lateral compositional modulation. Thus, short-period superlattice spots are expected along the surface-normal [001] direction. The [001] separation of the SPS satellites is $2\pi/p_{sps}$, where $p_{sps}$ is the period of the SPS. The net effect is 2-D compositional modulation in real-space (1-D spontaneous modulation along [110] and intentional SPS modulation along [001]) giving a 2-D network of satellites about each reciprocal lattice point.

In contrast to the $(GaP)_m(InP)_n$ and $(GaAs)_m(InAs)_n$ materials systems just discussed, lateral compositional modulation in $(AlAs)_m(InAs)_n$ SPSs grown on (001) InP tends to be 2-D in character. The in-plane modulation directions of the alternating Al-rich and In-rich domains vary with the net in-plane strain applied to the SPS by substrate coherency. Self-organization tends to occur along [100] and [010] for SPSs in net compression, or along [130] and [310] for SPSs in net tension [8, 9]. Again, some surface-normal SPS modulation persists in the laterally modulated structure. The net result for $(AlAs)_m(InAs)_n$ SPS growths is fully 3-D compositional modulation (spontaneous modulation along two in-plane directions and intentional SPS modulation along [001]). In this case, there is a corresponding 3-D network of superlattice satellites about each reciprocal lattice point.

Unlike our schematic, the actual intensities of the lateral-satellites vary for each reciprocal-lattice point and are given by Fourier transformation of the compositionally modulated real-space lattice. Glas [16] has calculated the elastic deformations of the lattice of an epitaxial layer whose intrinsic lattice parameter is sinusoidally modulated along the surface of the substrate on which it is grown. For layers thicker than the modulation wavelength, he finds that the bulk of the lateral superlattice is tetragonally strained like a normal superlattice, *but strain modulation is now transverse to the surface normal.* This symmetry change yields (00l) planes that have no modulation of their d-spacing; modulated displacements only occur parallel to (00l) planes.

Consequently, the scalar product, **K**·**r**, of the scattering vector, **K**, and the elastically deformed unit-cell lattice positions, **r**, produces no strain-related contributions to the lateral-satellite intensities for (002) and (004) reflections. The satellite intensities depend only on chemical modulations, which enter via the unit-cell structure factor. Satellite amplitudes are proportional to the amplitude of the locally varying binary-alloy mole fractions multiplied by the difference in the group-III atomic scattering factors. Weak (002) satellites result; they are observable because the comparably weak quasi-forbidden (002) fundamental produces low diffuse background allowing their detection. Weak (004) satellites also result; they are not easily observed because the very strong (004) fundamental produces a high diffuse background that obscures. In contrast to these symmetric reflections, asymmetric reflections introduce non-zero strain-related phase shifts via **K**·**r** that couple in contributions to the lateral-satellite intensities that are proportional to the structure factor of the fundamental. Satellites about (224), which is not a quasi-forbidden reflection, are thus stronger. We observe no (004) lateral satellites, weak (002) satellites, and stronger (224) satellites in laterally modulated SPSs.

Spontaneously formed lateral superlattices have many random variations in structure, and statistical treatments of kinematic diffraction theory are appropriate for detailed diffraction simulations. Darhuber et al. [21] present simulations of this type for self-organized arrays of quantum dots which partly resemble the present structures. Such detailed modeling is not the goal of the present work. We instead focus on using parameters easily extracted from maps: integrated lateral-satellite intensity, lateral-satellite and SPS-satellite periodicity, lateral-satellite vertical coherence length, SPS net strain and average composition, and in-plane coherence length. These parameters facilitate routine use of reciprocal-space maps to study variations in compositional modulation in SPS materials.

### 3. Reciprocal-space mapping using position-sensitive x-ray detection

Timely mapping of the diffuse x-ray diffraction produced by laterally inhomogeneous structure in epitaxial crystals is often difficult using traditional methods. As shown in Figure 2(a), the traditional approach for mapping reciprocal space by x-ray diffraction involves serial mechanical scanning in two dimensions. The sample crystal sequentially rotates through a series of rocking angles, $\omega_i$, i=1 to M. At each angle, $\omega_i$, the diffracted-beam-analyzer crystal and x-ray counter rotate through a series of x-ray scattering angles, $2\theta_j$, j=1 to N. At each ($\omega_i$, $2\theta_j$) the intensity of the analyzed diffracted beam is sampled for a counting time, Δt. The time required to complete a two-dimensional serial scan of the NxM array of angles required to make a reciprocal-space map is NxMxΔt.

Typical values for N, M, and Δt depend strongly on the apparatus, materials, research interests, and bent of the experimenter. We use an ordinary sealed-tube x-ray source monochromated to deliver ~$2.8\text{x}10^6$ Cu $K_{\alpha 1}$ x-rays/second. Most often we examine imperfect compound-semiconductor epitaxial layers that are typically ~100-5000 Å thick, and Δt values of 3 to 300 seconds are needed to make good-quality intensity measurements. A high-resolution map about a single reciprocal lattice point requires N and M between 100 and 400. In our case, serial scanning implies data-collection times ranging from 30,000 to $4.8\text{x}10^7$ seconds (8.3 hours to 1.5 years). These experiments are clearly impractical.

Dramatic reductions in scan time are achieved by coupling a position-sensitive x-ray detector (PSD) to the diffractometer in order to simultaneously measure all 2θ angles of interest [22]. As shown in Figure 2(b), the PSD replaces the analyzer crystal and x-ray counter and eliminates the need for serial scanning over 2θ. Assuming for the moment that all else is equal, the scan time is reduced to MxΔt. This is identical to the scan time required for a standard, one-dimensional, rocking curve made with an ordinary uncollimated detector; the PSD provides the scattering-angle information required to produce a two-dimensional reciprocal-space map with no increase in scan time. Typical scan times for the reciprocal-space maps that we collect using PSD-based diffractometry are ~300 to $1.2\text{x}10^5$ seconds (5 minutes to 33.3 hours).

PSD-based measurements of 2θ entail important tradeoffs -- all is in fact not equal. For example, the PSD used here is a gas-filled proportional counter; a 25-μm-diameter resistive-anode wire encodes the x-ray position. The potential for wire damage at high point-loaded count rates lowers the dynamic range of the PSD relative to that of a standard x-ray counter. Accommodation of the lower dynamic-range requires modulation of the incident-beam intensity when scanning through intensely diffracting structures. The reader will see reduced-intensity streaks through the substrate peaks in our maps resulting from this intensity-modulation requirement. A more important drawback of PSD use is reduced 2θ resolution. The present PSD-based 2θ measurements have a FWHM resolution of 160 arc-seconds versus ~12 arc-seconds for a modern high-resolution diffractometer using (220) Ge crystals throughout. A second-generation PSD-based instrument is now under development at Sandia National Laboratories, which will improve both 2θ resolution and dynamic range. PSD-based reciprocal-space mapping is discussed further in reference [22].

## 4. Parametric variations in compositional modulation

The relative speed afforded by use of a PSD enables routine application of two-dimensional mapping -- we applied this technique in a parametric study of the conditions required to produce compositional modulation during SPS growth. Variations in compositional modulation due to systematic changes in the average composition, the period, and the growth rate of $(AlAs)_m(InAs)_n$ SPSs are reported, but first we give some preliminaries.

The SPS period is defined by $p_{sps}$=n+m, where m and n are the ML-thicknesses of the AlAs and InAs layers, respectively, that form each period. The average InAs composition of the SPS is x=n/(n+m). Parameters were varied about a standard reference SPS structure and a standard set of growth conditions. The reference structure was a 100-period $(AlAs)_{2.00}(InAs)_{1.85}$ SPS, deposited on a lattice-matched 1800-Å-thick $Al_{0.48}In_{0.52}As$ random-alloy buffer, which was in turn deposited on a semi-insulating (001) InP substrate. The standard growth temperature was 530 °C for both buffer and SPS. The standard growth rate was ~0.35 ML/s for either AlAs or InAs growth on InP. During SPS deposition, these rates required the indium and aluminum cell shutters to sequentially operate approximately every 5 to 6 seconds to produce alternating growths of each binary alloy.

### 4.1 Variation with average composition

A series of SPS samples with average InAs mole fractions ranging from x=0.40 to x=0.68 were grown. The original intent of the series was to maintain the SPS period constant at the reference value of 3.85 ML while varying the InAs mole fraction about the lattice-matched condition x=0.522. For SPS samples grown indium-poor with x<0.522 this was successfully accomplished by reducing n while raising m. Observation of streaky RHEED patterns during these net-tensile SPS growths indicated a 2-D growth mode. For SPS samples grown indium-rich the constant-periodicity scheme failed. As x was increased beyond ~0.55 (n~2.1 ML, m~1.7 ML) growth entered a rough 3-D regime as indicated by spotty RHEED patterns. Subsequent indium-rich, net-compressive, SPS samples in the series were grown with n+m variable and with n<2 ML in order to maintain 2-D growth. The SPS period thus varies from 3-to-4 ML for the series.

Compositional modulation in each sample was characterized using (002) reciprocal-space maps acquired as $[\bar{1}10]$ zone-axis projections. Typical (002) maps for SPS samples with and without lateral compositional modulation appear in Figure 3. These two samples were also examined by TEM; plan-view and cross-sectional images appear in reference [9]. Figure 3(a) shows the map of sample EA0121, which has no detectable lateral satellites. TEM images of this sample show an SPS with very weak lateral compositional contrast consistent with laterally homogeneous SPS growth. Figure 3(b) shows the map of sample EA0122, which has strong lateral satellites. TEM images of this sample show strong, periodic, dark-light contrast characteristic of lateral compositional modulation. The 24 nm lateral-satellite period seen in the reciprocal-space map of Figure 3(b) agrees with the 20 nm modulation period seen in TEM images. Thus, direct comparisons of reciprocal-space maps with TEM images confirm that the observed lateral satellites reliably indicate the occurrence of compositional modulation.

The maps shown in Figure 3 used the full ω-range accessible in a single scan with our goniometer. A goal of these scans was to simultaneously view satellites due to both the lateral-superlattice and the SPS. To achieve this goal and view the -1 SPS satellite within the available ω-scan limits, we sacrificed measurement of the positive-numbered lateral satellites. Measurement of the -1 SPS satellite gave a post-growth measurement of the period of the SPS for comparison with pre-growth RHEED calibrations. RHEED and x-ray diffraction measurements of the

SPS period agreed to within a root-mean-squared error of ±0.06 ML, indicating that shutter-transient effects during the SPS deposition were small.

The net integrated intensity of the (002) -1 lateral satellite indicates the relative degree of compositional modulation. All maps were acquired under similar conditions, and net satellite intensities were obtained by subtracting off a diffuse-scattering background obtained by mapping structurally similar, unmodulated SPS samples. Since the number of SPS periods was maintained constant at 100, the total number of deposited monolayers varies with n and m for each sample. Thus, the intensity data were normalized by dividing by the SPS ML-thicknesses.

Parametric trends in the compositional modulation were examined by plotting the relative integrated intensity versus various parameters of interest (e. g., average composition, net in-plane strain of the SPS, n, m, and n+m). For instance, a plot of the (002) lateral-satellite intensity versus InAs mole fraction is shown in Figure 4. Compositional modulation peaks when the average composition of the SPS is approximately equal to that of the lattice-matched random alloy. Variations of the average InAs mole fraction exceeding ±0.10 completely suppress the occurrence of the spontaneous modulation. While spontaneous compositional modulation occurs in a well-defined window of average alloy compositions, average composition is not the sole pivotal factor; the SPS period also plays a key role.

### 4.2 Variation with SPS Period

Short-period superlattice samples with nominal periods of 1.0, 2.0, 2.8, 3.0, and 4.0 ML were grown. The average InAs mole fraction for the series was x=0.486. The variance of the composition for this series was higher than desired at ±0.023; nonetheless, the data of Figure 4 indicates that all of the compositions for this series should lead to observable compositional modulation when the SPS period is near 4 ML. Here, compositional modulation was characterized using (224) reciprocal-space maps acquired as $[\bar{1}10]$ zone-axis projections. Figure 5 shows maps for the endpoint samples of the periodicity series. TEM images of these samples again appear in reference [9] for comparison.

As an aside, consider the (002) map and sample of Figure 3(b) and the (224) map and sample of Figure 5(a); the two samples are almost alike so we compare their maps. Moving from (002) to (224) we find simple but important signatures which further confirm that the lateral satellites arise from in-plane correlation effects. For both reciprocal-lattice points the observed satellites remain aligned along [110]; moreover, the satellite spacing in both maps is nearly equal. Both observations are as expected for satellites arising from a lateral superlattice.

Returning now to periodicity effects, the 4.0-ML-period-sample map in Figure 5(a) shows distinct lateral satellites indicating strong compositional modulation. The 3.0-ML-period-sample map has lateral satellites of similar intensity. Corresponding TEM images show strong, periodic, dark-light contrast characteristic of compositional modulation and again consistent with the present lateral-satellite observations.

In contrast, both the 2.8- and 2.0-ML-period samples have weak lateral satellites; integrated intensities are ~0.15 times that of the 3.0- and 4.0-ML samples. Remarkably, a very small change in the SPS period from 3.0 to 2.8 ML (at nominally fixed composition) leads to a more than fivefold reduction in the compositional modulation. TEM of the 2.0-ML sample shows much-diminished modulating contrast consistent with the weaker lateral satellites.

Finally, the 1.0-ML-period-sample map in Figure 5(b) shows no lateral satellites indicating further reduction in the compositional modulation; TEM does, however, show some remnant of weak lateral contrast. The 1.0-ML sample may be weakly modulated at a level detectable by TEM but below the detection limits of the present reciprocal-space maps. Broadening of the 1.0-ML-period-sample reflections is seen in Figure 5(b); this is due to an incipient dislocation array. The overall results for the periodicity series indicate that at fixed average composition the degree of compositional modulation depends strongly on the SPS period.

### 4.3 Variation with average growth rate

Short-period superlattice samples were grown using average growth rates of 0.501, 0.361, 0.251 and 0.176 ML/s. The lowest rate was obtained using our standard-SPS-growth procedure, but with fully shuttered growth interrupts added to produce a 50% duty cycle. All other samples were grown under continuous deposition of either In or Al species with rate variations obtained by changing the In and Al effusion-cell temperatures.

The effect of average growth rate on compositional modulation was again monitored using (224) reciprocal-space maps acquired as $[\bar{1}10]$ zone-axis projections. Strong lateral satellites are seen in maps of all samples in this series; for growth at 530 °C, all growth rates examined led to lateral compositional modulation. Example maps for samples grown with the highest and lowest average growth rates appear in Figure 6.

The maps of the growth-rate series show a striking trend: the lateral-satellites monotonically increase in width along $K_\perp$ as the growth rate decreases. The FWHM satellite width, $w_\perp$, is inversely related to the vertical length of the lateral domains in the SPS by $L_\perp \sim 2\pi/w_\perp$. Thus, the increasing satellite widths indicate shorter coherent domains and degraded vertical self-alignment of the modulation as the growth rate decreases. We estimated the domain lengths using values for $w_\perp$ obtained from the +1 lateral satellites; figure 6 shows the vertical length of the modulated domains varying from 73 nm at the highest growth rate downward to 28 nm at the lowest growth rate. Cross-section-TEM images of samples from the growth-rate series once more appear in reference [9]. The images quantitatively confirm the domain lengths extracted from the reciprocal-space maps.

## 5. Recapitulation

Spontaneous compositional modulation occurs along the growth front during molecular-beam epitaxy of $(AlAs)_m(InAs)_n$ short-period superlattices. The modulation is quasi-periodic and forms a lateral superlattice superimposed on the intended SPS structure. Corresponding transverse satellites arise about each reciprocal lattice point, and x-ray diffraction can be routinely used to map their local reciprocal-space structure. The integrated intensity, spacing, orientation, and shape of these satellites provide a reliable means for nondestructively detecting and characterizing the compositional modulation in short-period superlattices. The analytical efficiency afforded by the use of a PSD has enabled detailed study of systematic variations in compositional modulation as a function of the average composition, the period, and the growth rate of the short-period superlattice.

## Acknowledgments

The Division of Materials Sciences in the Office of Basic Energy Sciences of the United States Department of Energy (DOE) supported this work under contract DE-AC04-94A185000. Lockheed-Martin operates Sandia National Laboratories for the DOE. Midwest Research Institute operates the National Renewable Energy Laboratory for the DOE.

Sandia is a multiprogram laboratory
operated by Sandia Corporation, a
Lockheed Martin Company, for the
United States Department of Energy
under contract DE-AC04-94AL85000.

## References

1. K. C. HSIEH, J. N. BAILLARGEON and K. Y. CHENG, Appl. Phys. Lett. **57** (1990) 2244.
2. K. Y. CHENG, K. C. HSIEH and J. N. BAILLARGEON, Appl. Phys. Lett. **60** (1992) 2892.
3. J. MIRECKI MILLUNCHICK, R. D. TWESTEN, D. M. FOLLSTAEDT, S. R. LEE, E. D. JONES, YONG ZHANG, S. P. AHRENKIEL and A. MASCARENHAS, Appl. Phys. Lett. **70** (1997) 1402.
4. R. D. TWESTEN, J. M. MILLUNCHICK, S. P. AHRENKIEL, Y. ZHANG, S. R. LEE, D. M. FOLLSTAEDT, A. MASCARENHAS and E. D. JONES, in Mat. Res. Soc. Symp. Proc. Vol. **441**, edited by S. C. Moss et al. (MRS, Pittsburgh, 1997) p. 187.
5. R. D. TWESTEN, et al., manuscript submitted.
6. A. C. CHEN, A. M. MOY, L. J. CHOU, K. C. HSIEH and K. Y. CHENG, Appl. Phys. Lett. **66** (1995) 2694.
7. S. T. CHOU, K. Y. CHENG, L. J. CHOU and K. C. HSIEH, J. Appl. Phys. **78** (1995) 6270.
8. A. G. NORMAN, S. P. AHRENKIEL, H. MOUTINHO, M. M. AL-JASSIM, A. MASCARENHAS, J. MIRECKI MILLUNCHICK, S. R. LEE, R. D. TWESTEN, D. M. FOLLSTAEDT, J. L. RENO and E. D. JONES, Appl. Phys. Lett. **73** (1998) 1844.
9. S. P. AHRENKIEL, A. G. NORMAN, M. M. AL-JASSIM, A. MASCARENHAS, J. MIRECKI MILLUNCHICK, R. D. TWESTEN, S. R. LEE, D. M. FOLLSTAEDT and E. D. JONES, to be published in J. Appl. Phys. **84** (1998).
10. YONG ZHANG and A. MASCARENHAS, Phys. Rev. B **57** (1998) 12245.
11. S. T. CHOU, D. E. WOHLERT, K. Y. CHENG and K. C. HSIEH, J. Appl. Phys. **83** (1998) 3469.
12. A. MASCARENHAS, Y. ZHANG, J. MIRECKI MILLUNCHICK, R. D. TWESTEN and E. D. JONES, AIP Conf. Proc. **404** (1997) 303.

13. PAUL J. PEARAH, ARNOLD C. CHEN, AARON M. MOY, KUANG-CHIEN HSIEH and KEH-YUNG CHENG, IEEE J. Quantum Electron. **30** (1994) 608.

14. JOHN W. CAHN, Acta Met. **9** (1961) 795.

15. G. B. STRINGFELLOW, J. Electron. Mater. **11** (1982) 903.

16. FRANK GLAS, J. Appl. Phys. **62** (1987) 3201.

17. FRANK GLAS, Phys. Rev. B **55** (1997) 11277.

18 J. E. GUYER and P. W. VOORHEES, J. Cryst. Growth **187** (1998) 150.

19 I. P. IPATOVA, V. G. MALYSHKIN, A. A. MARADUDIN, V. A. SHCHUKIN and R. F. WALLIS, Phys. Rev. B **57** (1998) 12968.

20 J. MIRECKI MILLUNCHICK, R. D. TWESTEN, S. R. LEE, D. M. FOLLSTAEDT, E. D. JONES, S. P. AHRENKIEL, Y. ZHANG, H. M. CHEONG and A. MASCARENHAS, MRS Bulletin **22** (July 1997) Number 7, p. 38.

21. A. A. DARHUBER, J. STANGL, V. HOLY, G. BAUER, A. KROST, M. GRUNDMANN, D. BIMBERG, V. M. USTINOV, P. S. KOP'EV, A. O. KOSOGOV and P. WERNER, Thin Solid Films **306** (1997) 198.

22. S. R. LEE, B. L. DOYLE, T. J. DRUMMOND, J. W. MEDERNACH and R. P. SCHNEIDER JR., in "Advances in X-Ray Analysis, Vol. 38", edited by P. Predecki et al. (Plenum Press, NY, 1995) p. 201.

## Figure Captions

*Figure 1* (a) The real-space structure of an SPS with lateral modulation of the alloy composition. (b) The corresponding reciprocal-space structure. Black squares represent the reciprocal lattice of the substrate and lattice-matched buffer. White circles represent the reciprocal lattice of a coherently strained alloy having the average composition of the SPS. Light-grey circles along [001] represent first-order SPS satellites. Dark-grey circles along [110] represent transverse satellites due to compositional modulation.

*Figure 2* Two approaches for mapping reciprocal space: (a) traditional two-dimensional serial scanning of both $\omega$ and $2\theta$, (b) the PSD-based approach serially scans in only one dimension: $\omega$.

*Figure 3* (002) reciprocal-space maps of $(AlAs)_m(InAs)_n$ SPSs: (a) Sample EA0121: $p_{sps}=3.78$ ML, m=2.18 ML, n=1.60 ML, x=0.422; (b) Sample EA0122: $p_{sps}=3.98$ ML, m=2.13 ML, n=1.85 ML, x=0.466.

*Figure 4* Integrated intensity of the (002) lateral-satellite versus the average InAs mole fraction of the SPS.

*Figure 5* (224) reciprocal-space maps of $(AlAs)_m(InAs)_n$ SPSs: (a) Sample EA0184 has a 3.93 ML period with m=1.95 ML, n=1.98 ML and x=0.505; (b) Sample EA0183 has a 1.02 ML period with m=0.56 ML, n=0.47 ML and x=0.456.

*Figure 6* (224) reciprocal-space maps of $(AlAs)_m(InAs)_n$ SPSs: (a) Sample EA0187 was grown at 0.50 ML/s with m=2.05 ML, n=1.90 ML and x=0.481; (b) Sample EA0186 was grown at 0.18 ML/s with m=1.80 ML, n=1.72 ML and x=0.488.

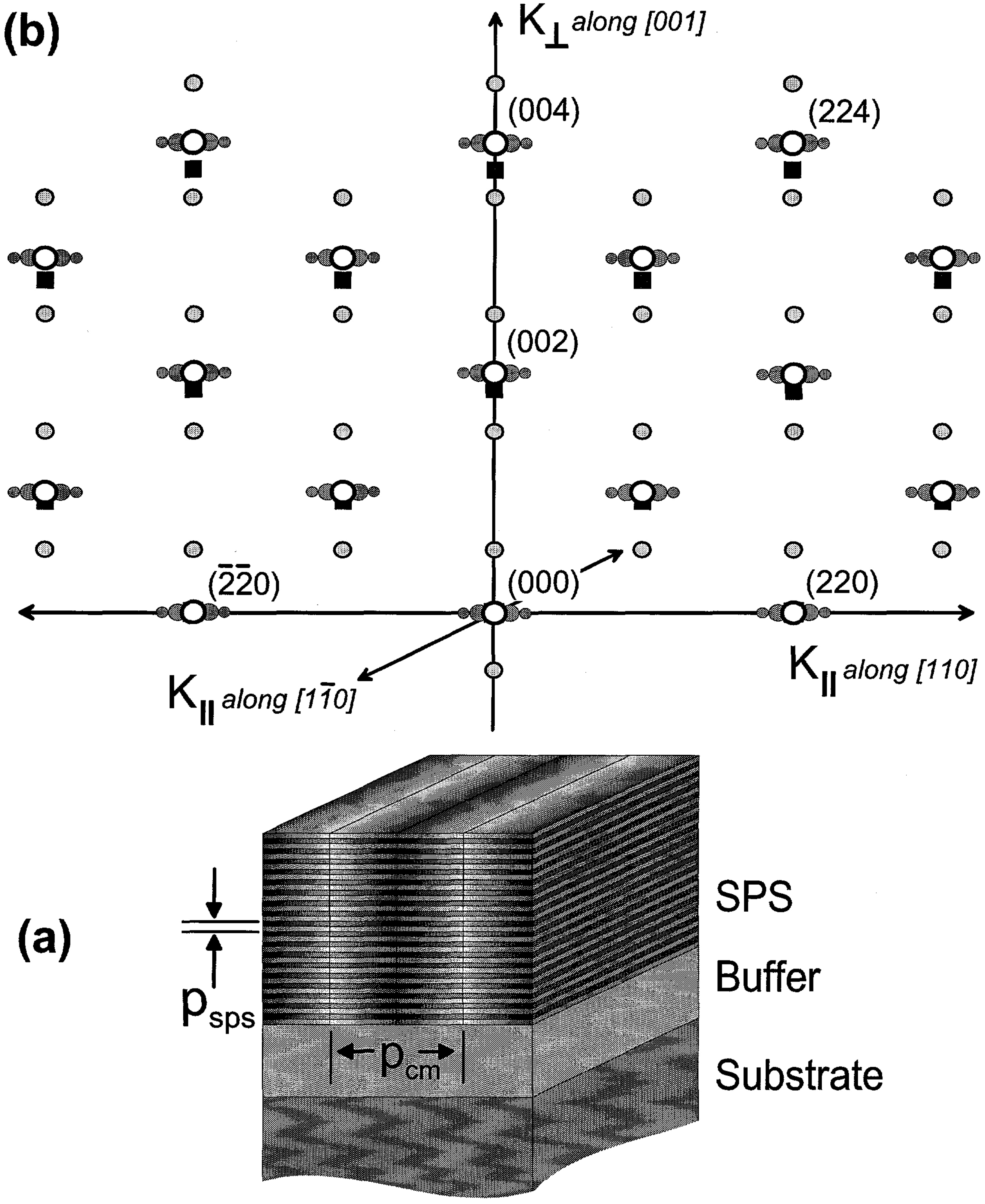

Lee et al.,
Figure 1

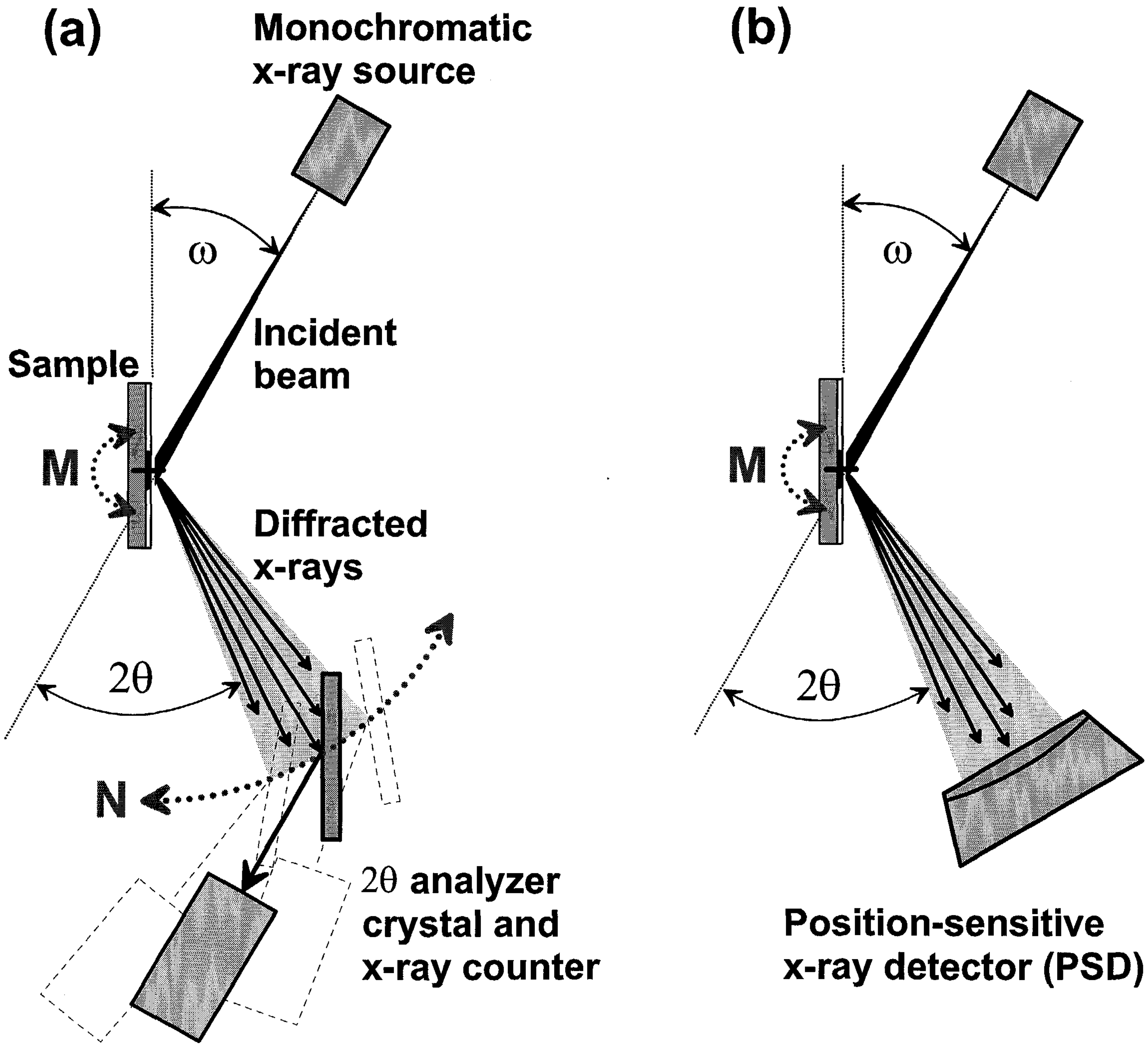

Lee et al.,
Figure 2

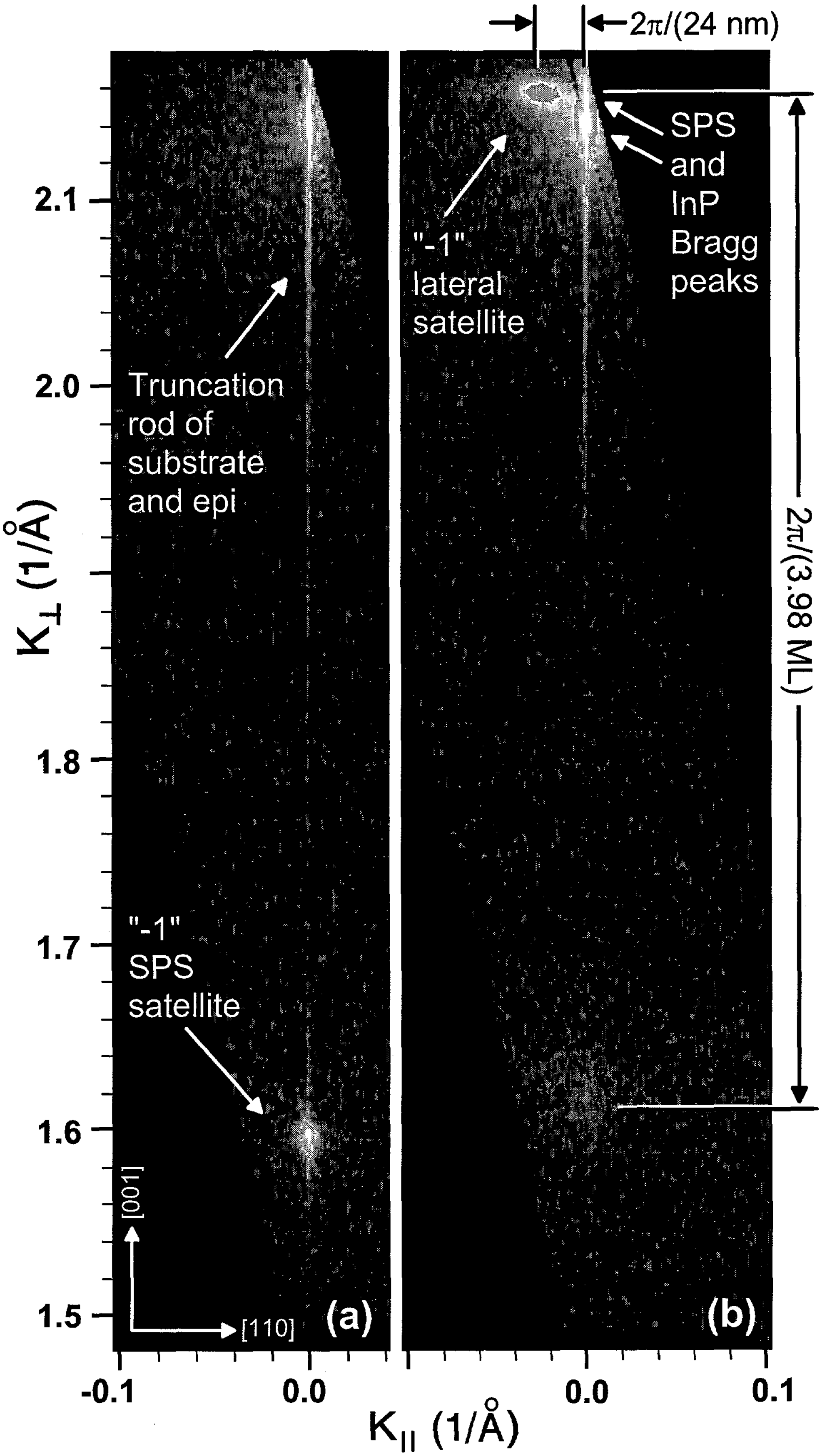

Lee et al.,
Figure 3

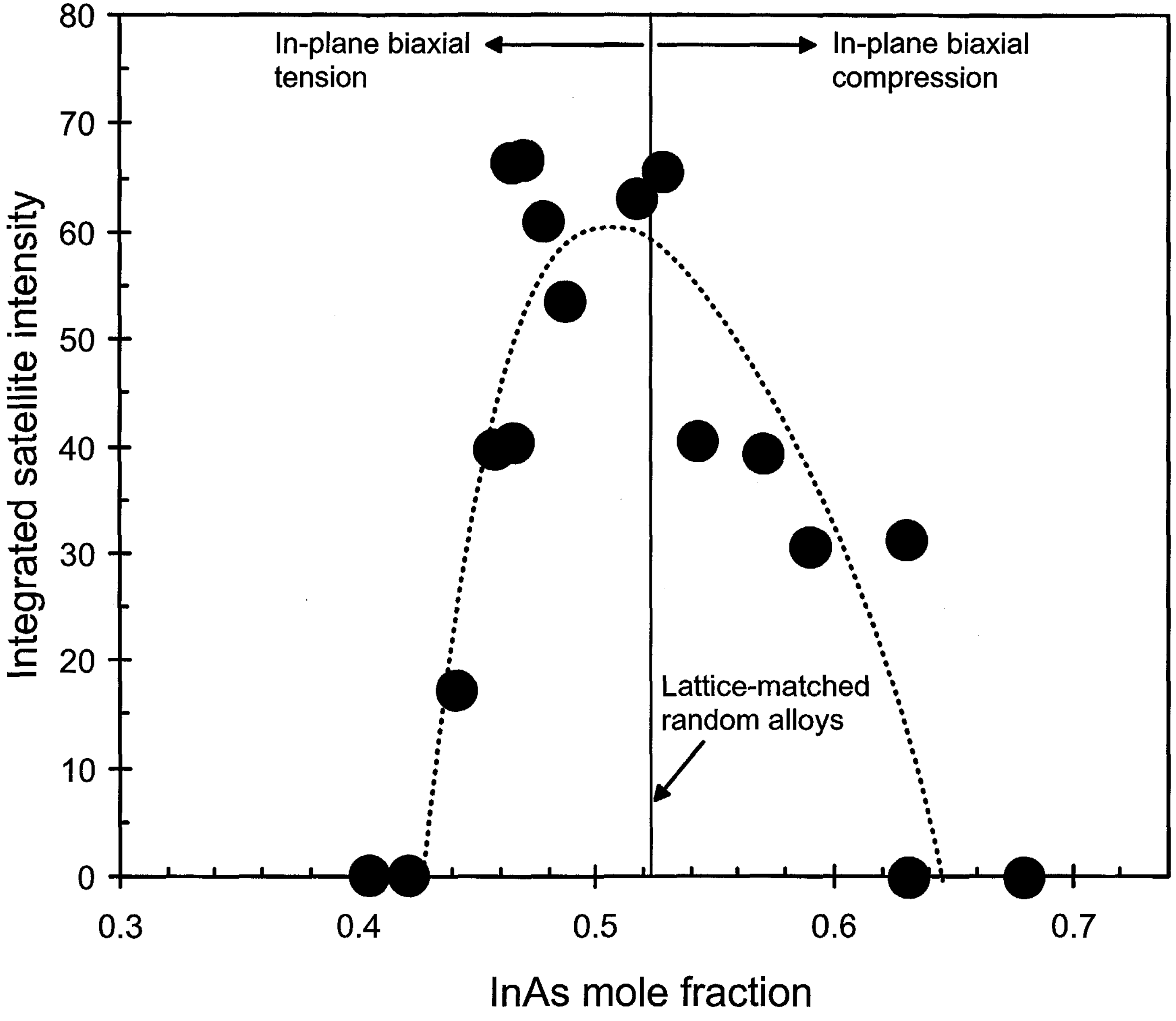

Lee et al.,
Figure 4

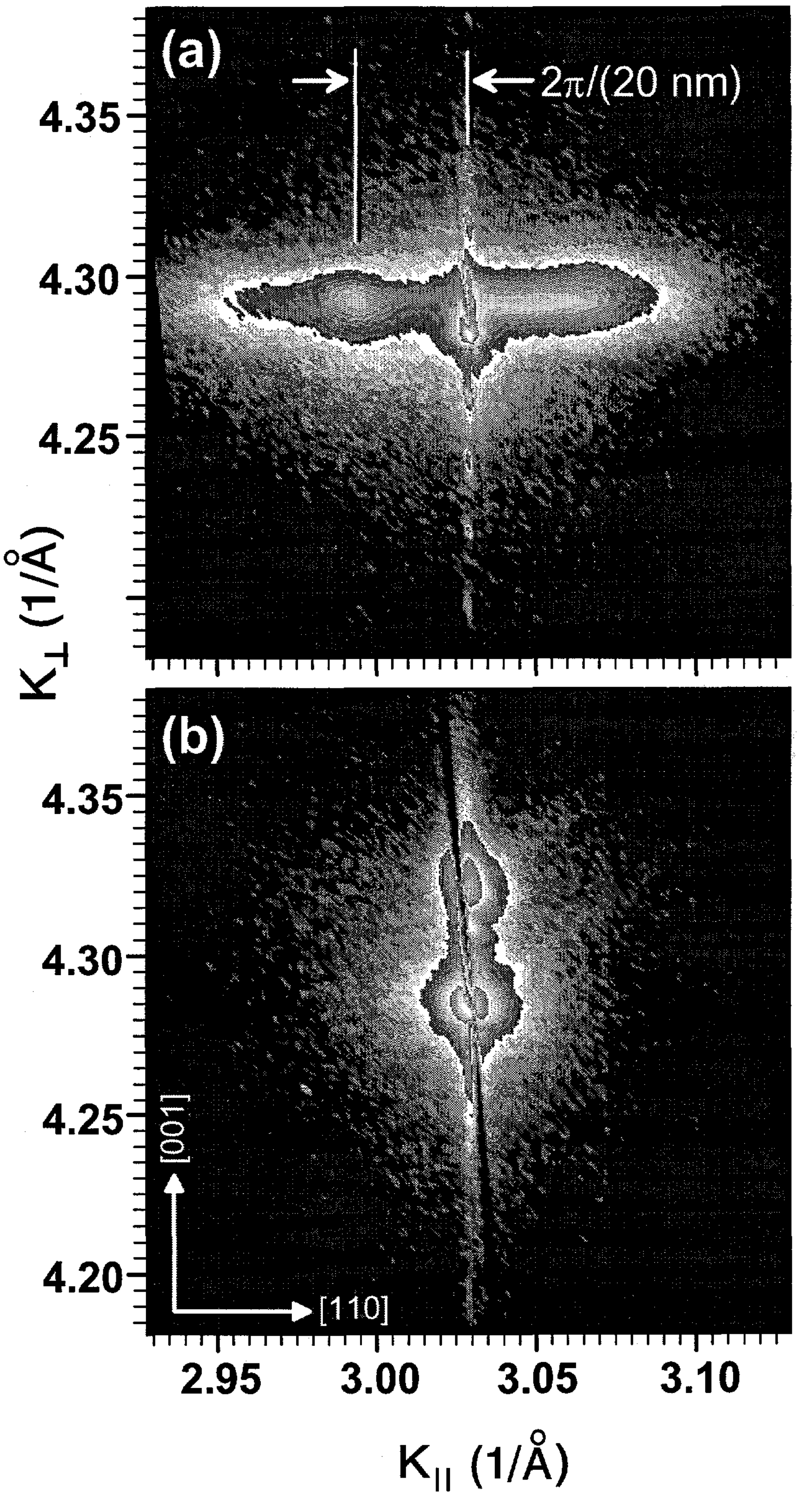

Lee et al.,
Figure 5

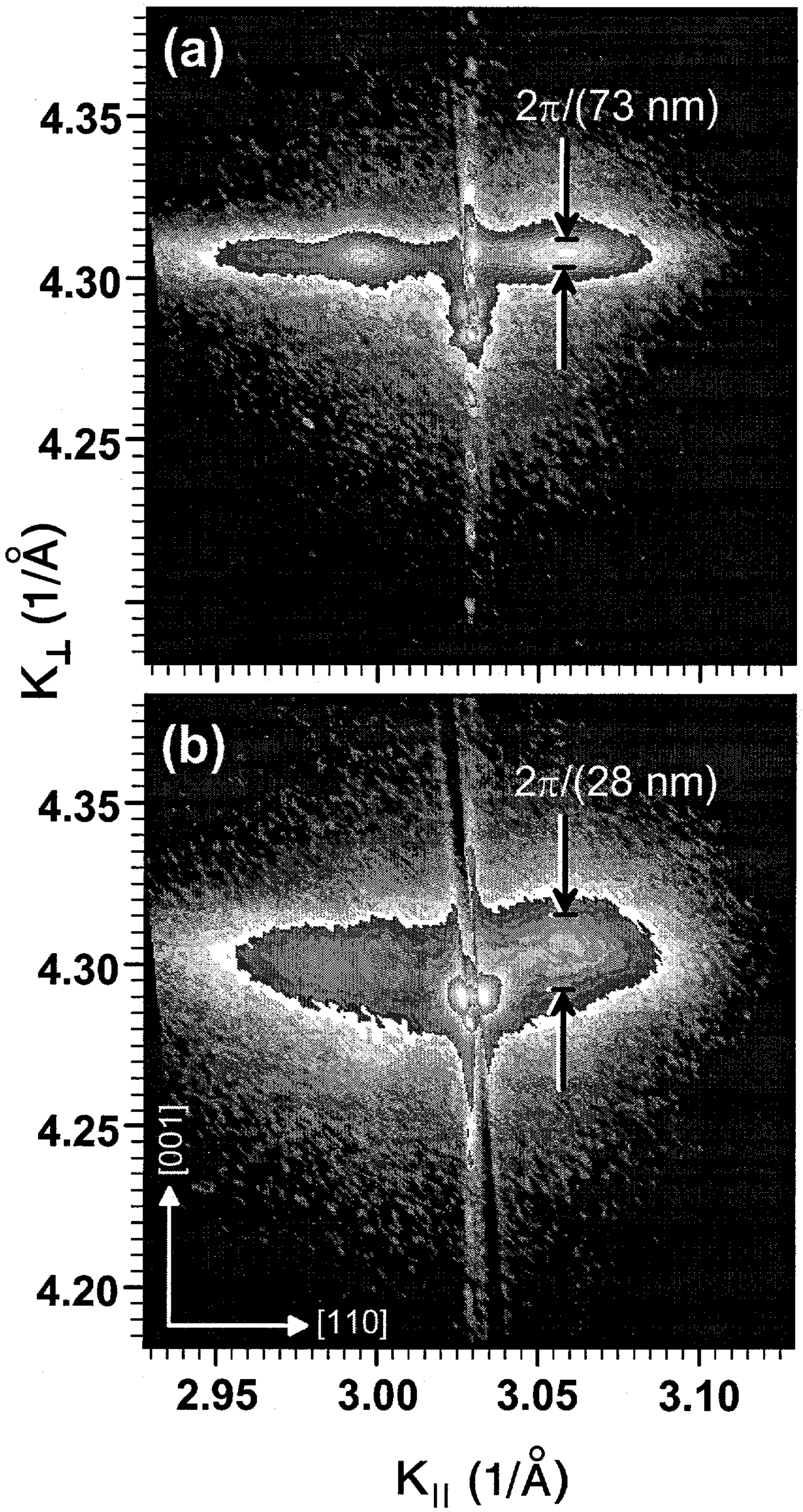

Lee et al.,
Figure 6